16th ICAAR LISBOA 2020-2022

16th International Conference on
Alkali-Aggregate Reaction in Concrete
Lisboa | LNEC | Portugal | 31 May - 2 June 2022

http://icaar2020-2022.lnec.pt

ASR expansions modelling under multi-axial stresses

P. Morenon [1,2], S. Multon [1], A. Sellier [1]

(1) Université de Toulouse, UPS, INSA, LMDC (Laboratoire Matériaux et Durabilité des Constructions), 135, avenue de Rangueil, F-31 077 Toulouse Cedex 04, France

(2) Toulouse Tech Tranfer, 118 route de Narbonne, CS 24246, 31432 Toulouse Cedex 04, France

Abstract

A lot of structures affected by Alkali-Silica Reaction (ASR) are submitted to anisotropic stress or restrained states. ASR expansion under external loadings and restraints leads to anisotropic cracking. In such conditions, the expansion and resulting cracking are lower or non-existent in the restrained direction. A higher deformation than the one observed in free swelling can be obtained in the unrestrained directions.

Numerous models have been developed to predict structural behaviour and several recent experiments [1, 2] on ASR swellings submitted to multi-axial stresses can be used to validate existing models. Indeed, the literature already contains many cases with uniaxial loadings but few experiments present ASR under real multi-axial loadings. In these new tests, multi-axial loadings have been applied to simple geometry samples (in addition to stress free expansion tests and uniaxial loading). Furthermore, new ways to apply these mechanical conditions are used such as post-tensioning bolts or triaxial machine. However, the analysis stays complex due to the combination with concrete damage and creep.

To ensure the safety of large ASR affected structures, numerical models must integrate these phenomena. In this paper, a poromechanical model which takes into account anisotropy, creep and multi-axial loadings is applied to these new experiments.

***Keywords**: anisotropy; expansion; modelling; multi-axial stresses*

1. INTRODUCTION

Many structures affected by Alkali-Silica Reaction (ASR) are submitted to external multiaxial loadings or restraints. They affect the swelling and lead to anisotropic strains and cracking in case of anisotropic stress state. Thus, the cracking is mainly along longitudinal reinforcement in reinforced beams affected by ASR. The expansion in the free directions can be equal or greater than the one obtained in a stress-free swelling test. Under triaxial loading, the volumetric ASR expansion is strongly reduced but not totally cancelled [1].

A few experimental tests were performed to quantify the behaviour of ASR affected concrete in such multi-axial conditions [3]. Recently, two important works were published on this subject [1, 2]. Based on the work all-ready done in [4], a poromechanical model which takes into account creep, ASR gel pressure and anisotropic damage is applied to these experiments in order to show its abilities and limits.

2. POROMECHANICAL MODELLING

The model used to reproduce ASR expansion under multi-axial stresses is based on the poromechanical framework [5]. The poromechanical effective stress $\tilde{\sigma}_{ij}{}'$ derives from the poromechanical total stress $\tilde{\sigma}_{ij}$ in the solid undamaged zone and the stress induced by the pressure P_g (Equation (1)).

$$\tilde{\sigma}_{ij} = \tilde{\sigma}_{ij}{}' - b_g P_g \quad (1)$$

with b_g, the Biot coefficient.

The damage induced by ASR expansion is modelled with a plasticity modelling strongly coupled with creep (Figure 2-1).

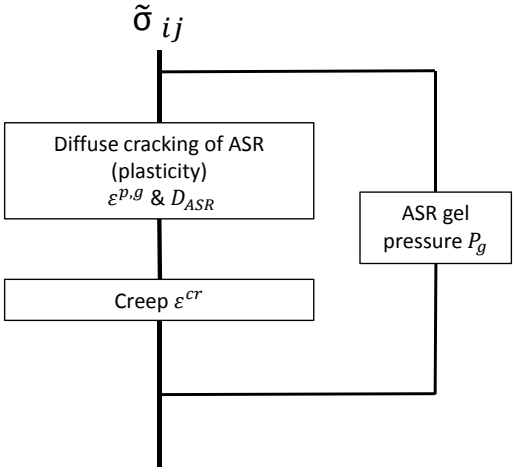

Figure 2.1: Poromechanical scheme [6]

2.1 ASR advancement

ASR advancement, A^{asr}, (Equation (2)) depends on:

- a characteristic time, τ_{ref}^{asr}, which can be calibrated on a free expansion test,
- the temperature T through the coefficient $C^{T,asr}$ which includes an Arrhenius law (Equation (3) with E^{asr} the thermal activation energy, R the perfect gas constant and T_{ref} the reference temperature),
- the water saturation degree S_r thanks to $C^{W,asr}$ (Equation (4)) which depends on $S_r^{th,asr}$ (the minimum threshold to initiate the reaction) [7–9]. Poyet's law has been slightly modified to improve the reproduction of swelling under different moisture contents [6].
- $< \cdots >^+$ represents the positive part of the quantity.

$$\frac{\delta A^{asr}}{\delta t} = \frac{1}{\tau_{ref}^{asr}} C^{T,asr} C^{W,asr} < Sr - A^{asr} >^+ \tag{2}$$

$$C^{T,asr} = \exp\left(-\frac{E^{asr}}{R}\left(\frac{1}{T} - \frac{1}{T_{ref}}\right)\right) \tag{3}$$

$$C^{W,asr} = \begin{cases} \left(\frac{S_r - S_r^{th,asr}}{1 - S_r^{th,asr}}\right)^2 & if \quad S_r > S_r^{th,asr} \\ 0 & if \quad S_r \leq S_r^{th,asr} \end{cases} \tag{4}$$

2.2 Gel pressure

The volume of ASR gel, ϕ_g, is determined according to the advancement, A^{asr}, and to the final volume of gel, ϕ_g^∞, reached when the reaction is finished (Equation (5)):

$$\phi_g = \phi_g^\infty . A^{asr} \tag{5}$$

ϕ_g^∞ can be calibrated on a stress free expansion test.

The new products produced during ASR act on surrounding aggregate and cement paste as an internal pressure. The pressure comes from the difference of volume between the ASR-gels and the porosity connected to reactive sites and able to accommodate such new phases. This porosity can come from the initial local porosity (in aggregate and in cement paste) or from micro-cracking created by the gel

itself. In this work, the gel pressure P_g (Equation (6)) is evaluated from the volume of gel, ϕ_g, and from the volume accessible without swelling around the reaction site (ϕ_g^v):

$$P_g = M_g < \phi_g - \left(\phi_g^v \left(\frac{P_g}{\tilde{R}_I^t}\right) + b_g tr(\varepsilon^e + \varepsilon^{cr}) + tr(\varepsilon^{p,g})\right) >^+ \quad (6)$$

With M_g, the Biot modulus to evaluate the interaction between the gel and the concrete rigidities, $\tilde{R}_I^t$, the tensile strength, ε^e, the elastic strain, ε^{cr}, the creep strain and $\varepsilon^{p,g}$, the diffuse cracking induced by ASR.

2.3 Damage

2.3.1 ASR diffuse cracking

The stress state in concrete submitted to the internal pressure caused by ASR is mainly compression in radial direction and tension in ortho-radial direction around the reactive inclusions. It is consistent with the local reactive process without expansive gel diffusion out of connected porosity and cracks induced by ASR. If the gel pressure P_g is high enough, the microcracking begins in the ortho-radial direction around the inclusion. This phenomenon is translated by an ASR anisotropic plastic criterion in the model (Equation (7)) where $\tilde{\sigma}_I{}'$ is the effective poromechanical stress (Equation (8)) and $\tilde{R}_{t\,micro}$ is the effective tensile strength around the reactive site. In Equation (8), $\tilde{\sigma}_I$ is the external stress in the direction I. If there is an external compressive stress due to external loading, the microcracking is delayed or cancelled in this direction.

$$f_I^{t\,ASR} = \tilde{\sigma}_I{}' - \tilde{R}_{t\,micro} \quad I \in [I, II, III] \quad (7)$$

$$\tilde{\sigma}_I{}' = P_g + \min(\tilde{\sigma}_I\,; 0\,) \quad I \in [I, II, III] \quad (8)$$

After the first microcracking, the effective tensile strength $\tilde{R}_{t\,micro}$ increases. It represents the increase of the gel pressure necessary to propagate the microcrack in the aggregate and cement matrix (Figure 2-2). The slope of this effective tensile strength is managed by the hardening plastic coefficient h_g [4] (=0.03 from [4, 9]) and the concrete modulus E_c. It allows to obtain the ASR plastic strain $\varepsilon_I^{p,g}$ from the effective stress $\tilde{\sigma}_I{}'$. The hardening law has been calibrated on Multon's experimentations [3] in [4].

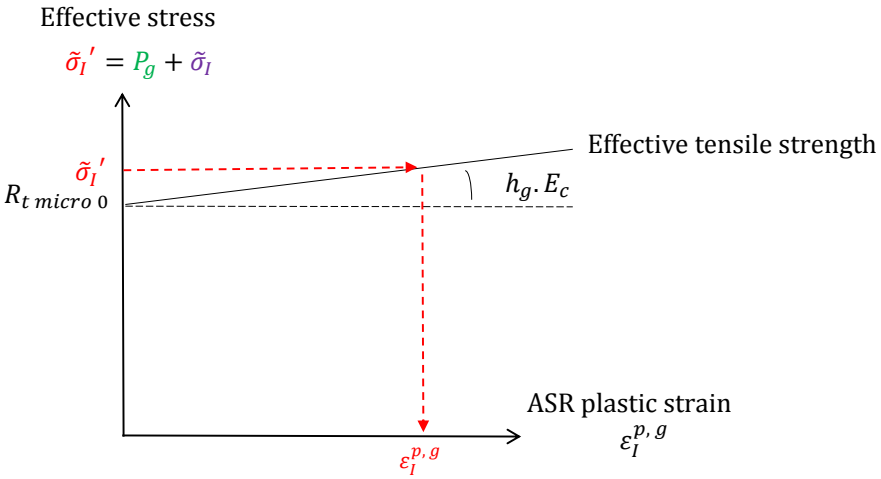

Figure 2.2: ASR anisotropic plastic criterion [4]

2.3.2 Structural localized cracking

In structures submitted to external loading or to expansion gradient, structural localized cracks can occur. In the model, it is managed by the combination with a damage modelling. The combination has been presented in [9]. In the present work, only specimens are analyzed and the impact of the structural damage is limited. As a consequence, it is not detailed in this paper.

2.4 Creep modelling

Sustained external or internal loadings lead to delayed strains. Shrinkage and creep strains are included directly in the poromechanical frame (Figure 2.1). The creep strain is composed of reversible creep (Kelvin-Voigt scheme Equation (9)) and permanent creep (Maxwell scheme Equation (10)).The permanent creep is managed by the consolidation theory [10].

In Equation (9), the increment of reversible creep strain $\partial\varepsilon_{ij}^{K}$ depends on a characteristic time τ^{K} (dependent on temperature and water content), the elastic strain ε_{ij}^{E}, the ratio between Kelvin-Voigt stiffness and the elastic modulus ψ^{K} and the reversible creep strain itself ε_{ij}^{K}.

In Equation (10), the increment of permanent creep strain $\partial\varepsilon_{ij}^{M}$ depends on a characteristic time τ_{ij}^{M} (dependent on temperature, water content and mechanical loading) and the elastic strain ε_{ij}^{E}.

$$\frac{\partial\varepsilon_{ij}^{K}}{\partial t} = \frac{1}{\tau^{K}}\left(\frac{\varepsilon_{ij}^{E}}{\psi^{K}} - \varepsilon_{ij}^{K}\right) \tag{9}$$

$$\frac{\partial\varepsilon_{ij}^{M}}{\partial t} = \frac{\varepsilon_{ij}^{E}}{\tau_{ij}^{M}} \tag{10}$$

3. ASR EXPANSIONS MODELLING UNDER MULTI-AXIAL STRESSES

Two different experiments of ASR expansions under multi-axial stresses are modelled here [1, 2]. For each one, the geometry, environmental conditions and load application conditions are described. The poromechanical model is calibrated on creep and free swelling experimental results. Then, swelling tests under multi-axial loadings are performed and compared to experimental results without supplementary calibration.

3.1 Modelling of Liaudat's experiments [1]

3.1.1 Geometry, environmental conditions and stresses applications

Liaudat's experiments were performed on 150 x 150 x 150 mm concrete cubes. After pouring, the samples were immersed in a 1 NaOH solution at 21°C during 3 months. The free swelling test was performed during 30 weeks. However, the triaxial loading tests were realised during 21 days. The temperature during the mechanical test was 60°C.

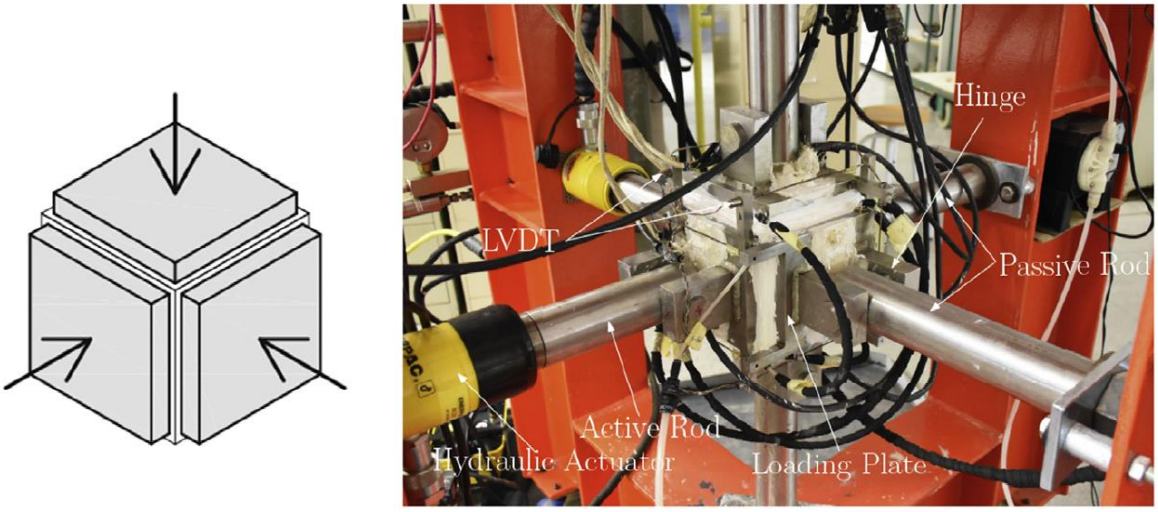

(a) (b)

Figure 3.1: Liaudat's experiment mechanical loading (a) scheme (b) picture of the set up

The stresses were directly applied by a triaxial load frame. To simplify the denomination of the tests, the following code is used. The first number corresponds to the X applied stress, the second to Y direction and the third to Z direction:

- Free swelling: 0-0-0 MPa
- Triaxial loadings: 1-1-1 MPa; 9-9-9 MPa; 9-9-1 MPa
- Triaxial loadings with stresses evolutions: 1-1-1 MPa during 22 days and then 1-1-9 MPa ; 9-9-9 MPa during 22 days and then 0-0-0 MPa.

As the conditions were quite homogeneous, the model is applied to a cube with only one finite element.

3.1.2 Modelling calibration

First, the creep of the poromechanical model is calibrated on non-reactive samples submitted to 1-1-1 MPa and 9-9-9 MPa (Figure 3.2 (a)). Then, the calibration of ASR parameters is only realised on the free sample results (Figure 3.2 (b) and detail of the first 30 days of swelling is given on the Figure 3.2 (c)). Only three parameters are fitted:

- the characteristic time of the ASR reaction $\tau_{ref}^{asr} = 450\ days$ (Equation (2)),
- the maximum volume of ASR gel $\phi_g^{\infty} = 0.4$ (Equation (5)).
- the volume reachable around the reaction site without swelling $\phi_g^{v} = 0.028$ (Equation (6)).

These values seem important but the experimental expansion is really high (2.5%) at 250 days for an ASR swelling. It could been due to the nature of aggregates (glass) and to the high alkali content. This laboratory concrete is very different from usual structural concrete. The glass aggregates are strongly consumed by ASR which can lead to a highly scalable porosity during the swelling process which does not so significant for usual concrete. In these conditions, the model could reach its limits that is why the parameters are amplified. Even if the physical meaning of the parameters can be questionable in this case, the mechanical response of the modelling is consistent with the experimental results.

At 8 days, the model slightly underestimates the strain compared to experimental results. Indeed, it seems that there is a strong expansion between 0 and 8 days. A water adsorption could be at the origin of this early expansion. Without experimental mass balance, it is not possible to calibrate its amplitude. Therefore, a better reproduction of the experimental data at 8 days is not wanted.

3.1.3 Comparison between experiment and modelling results

The results obtained on the triaxial loadings are presented on the Figure 3.2 (d,e,f). The model reproduced faithfully the kinetics and the amplitudes of the triaxial stress tests.

In the experimentations, the swelling is not reduced by the triaxial applied load of 1 MPa. Indeed, at 22 days, the expansion is 0.4% in this case (Figure 3.2, d) as for the stress free expansion test (Figure 3-2, c). At the opposite, the model predicts a slight decrease of expansion and thus overestimates the impact of the 1 MPa applied compressive stress compared to experimental results.

The ASR swelling is strongly weakened by the triaxial external applied stress of 9 MPa but expansions are not totally cancelled (Figure 3.2 (e)). The model reproduces this small expansion compared to the non-reactive concrete. During this phase, the creep and the ASR expansion are in competition to impact the direction of the strain evolution. For the 9-9-1 case, the swelling is mainly directed on the weakest load direction (Z). The model strain in the 1 MPa direction (Z) is well reproduced. The expansions in the other directions (X and Y) are slightly underestimated.

The Figure 3.3 shows the results obtained for the triaxial loadings with applied stresses evolutions. For the case from 1-1-1 MPa to 1-1-9 MPa (Figure 3.3 (a)) the model reduces the strain in the Z direction and rises the strains in the others. The amplitude of the phenomenon is quite well reproduced. For the 9-9-9 MPa to stress free swelling test (Figure 3.3 (b)), the model reproduces correctly the first phase. After the loading release, the model overestimates the kinetics of swelling. Indeed, in the model, the plastic criterion allows an instantaneous micro-cracking as soon as the external loading is removed. This assumption seems too severe. In the case of unloading, no instantaneous expansion is observed in the experimental results.

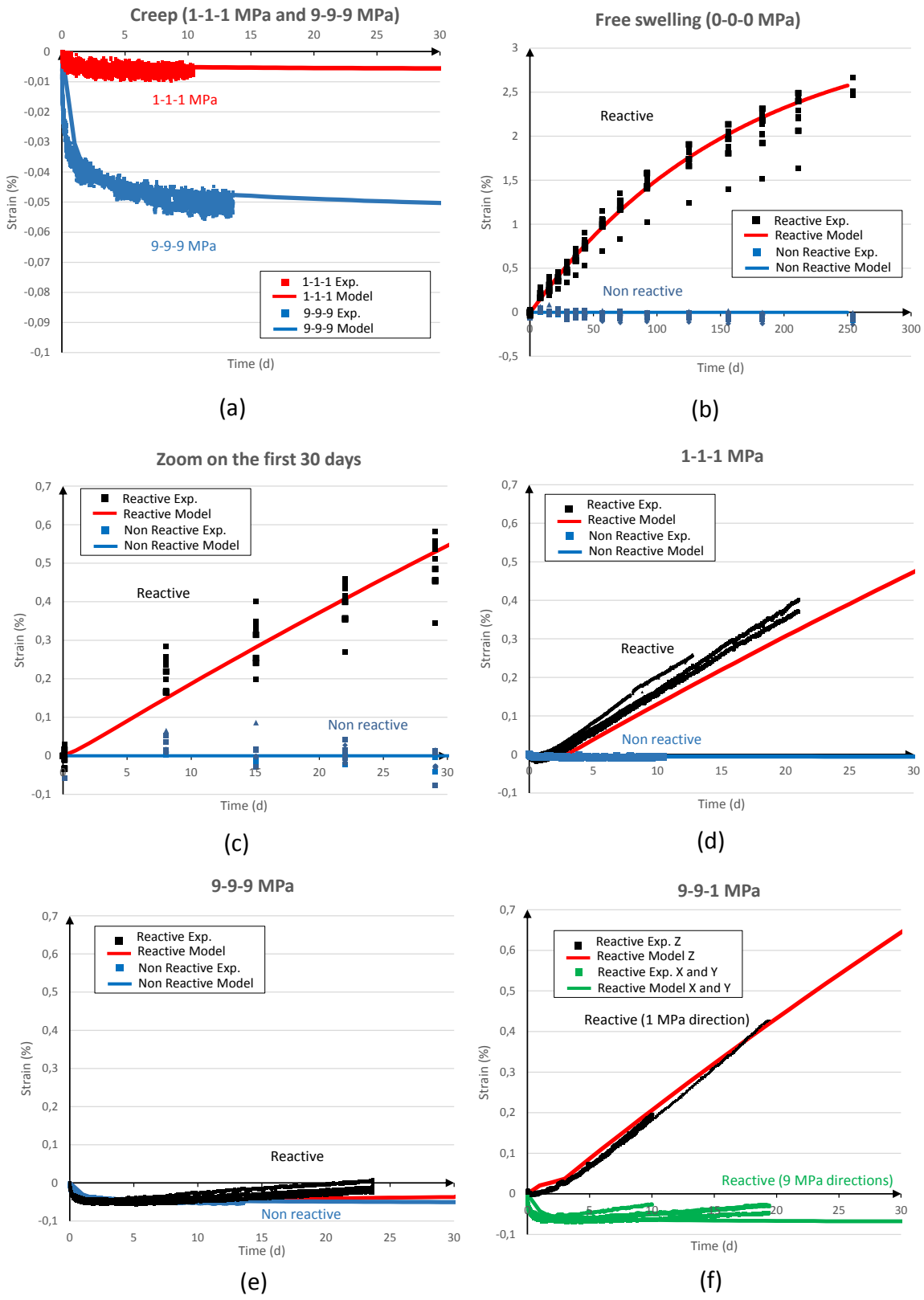

Figure 3.2: Calibration and comparison of the experiment results of [1] and the model results: (a) Triaxial non-reactive creep tests at 1 and 9 MPa (b) Calibration of the free swelling test (c) Zoom on the first 30 days of the free swelling test calibration (d) 1-1-1 MPa test comparision (e) 9-9-9 MPa test comparison (f) 9-9-1 MPa test comparision

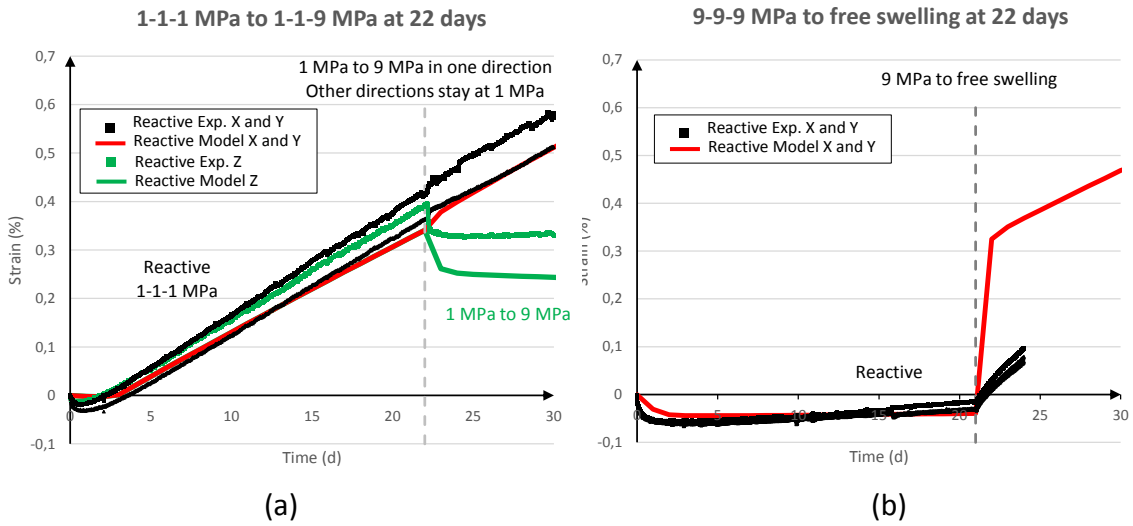

Figure 3.3: Comparison of the experiment results of [1] and the model results: (a) 1-1-1 MPa during 22 days and then 1-1-9 MPa (b) 9-9-9 MPa during 22 days and then free swelling

3.2 Modelling of Gautam's experiments [2]

3.2.1 Geometry, environmental conditions and stresses applications

Gautam's experiments were performed on 254 x 254 x 254 mm concrete cubes (Figure 3.4). Concrete cube specimens were submitted to multiaxial stresses using post-tensioning method of prestressing on high-strength bolts. The prestresses (3.9 MPa or 9.6 MPa in the concrete) were applied at an age of 52 to 56 days and during 500 days. Four steel plates were used to apply the stress from the bolts to the concrete on each face. The temperature was 23°C during the first 180 days after demolding, and then 50°C. The relative humidity was always higher than 95%.

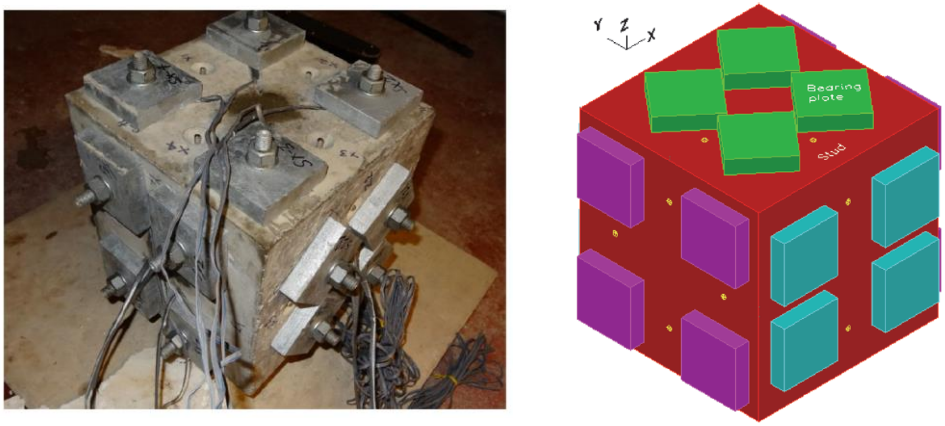

Figure 3.4: Photograph and multiaxial stress application arrangement in cube specimens [2, 11]

The stresses applied during the swelling tests were:

- Free swelling: 0-0-0 MPa
- Uniaxial loadings: 3.9-0-0 MPa and 9.6-0-0 MPa
- Biaxial loadings 3.9-3.9-0 MPa and 9.6-3.9-0 MPa
- Triaxial loadings: 3.9-3.9-3.9 MPa and 9.6-3.9-3.9 MPa

In the modelling, a displacement is applied at one side of the steel to reproduce the bolt prestressing.

Due to the strong heterogeneity of geometries on each loading test (the plates are more or less closed to the external edges of the specimen, the plates on Z direction are 40° rotated), the mesh has been reproduced in three dimensions (Figure 3.5). Only one eighth of the real cube is meshed because of symmetries.

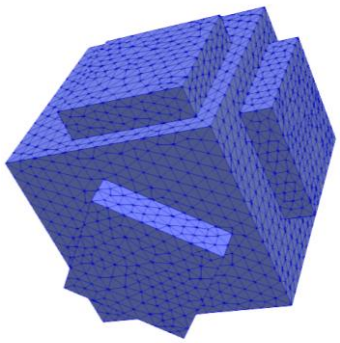

Figure 3.5: Mesh of 1/8 of the cube used for triaxial loadings simulations

3.2.2 Modelling calibration

The creep [10] is calibrated on two uniaxial tests (3.9 MPa and 9.6 MPa (Figure 3.6 (a)). As the loading was not sustained during time, it is not exactly a creep test, but the delayed strains thus obtained can be used to calibrate creep modelling. For the free swelling calibration, only three parameters are fitted (Figure 3.6 (b)):

- the characteristic time of the ASR reaction $\tau_{ref}^{asr} = 45\ days$ (Equation (2)),
- the maximum volume of ASR gel $\phi_g^{\infty} = 0.019$ (Equation (5)),
- the volume reachable around the reaction site without swelling $\phi_g^{v} = 0.0106$ (Equation (6)).

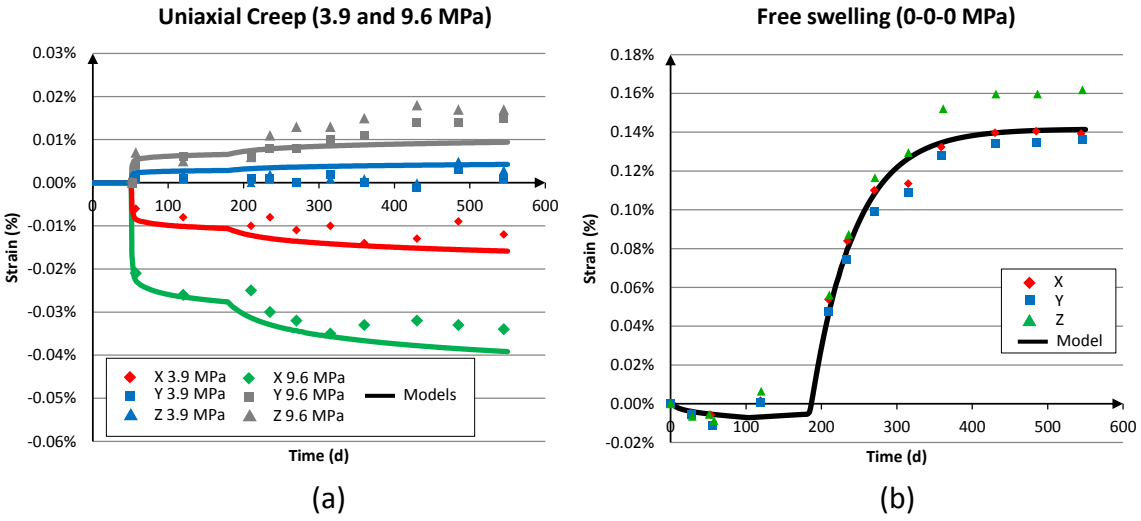

Figure 3.6: Calibrations of (a) the creep on two uniaxial tests (b) the free swelling [2]

3.2.3 Comparison between experiment and modelling results

All the expansions under multi-axial stresses are modelled (Figure 3.7). For the uniaxial tests (Figure 3.7 (a) and (b)), the strains are very well reproduced except for the loaded direction (X) in the 3.9-0-0 MPa test. In previous experimentations of the literature [4, 12, 13], a free swelling of 0.14% is usually strongly reduced by a uniaxial loading of 3.9 MPa in the loaded direction. It is not the case here as the reduction is only of about 30% (Figure 3-7 (a)). Globally, the multiaxial tests are reproduced faithfully.

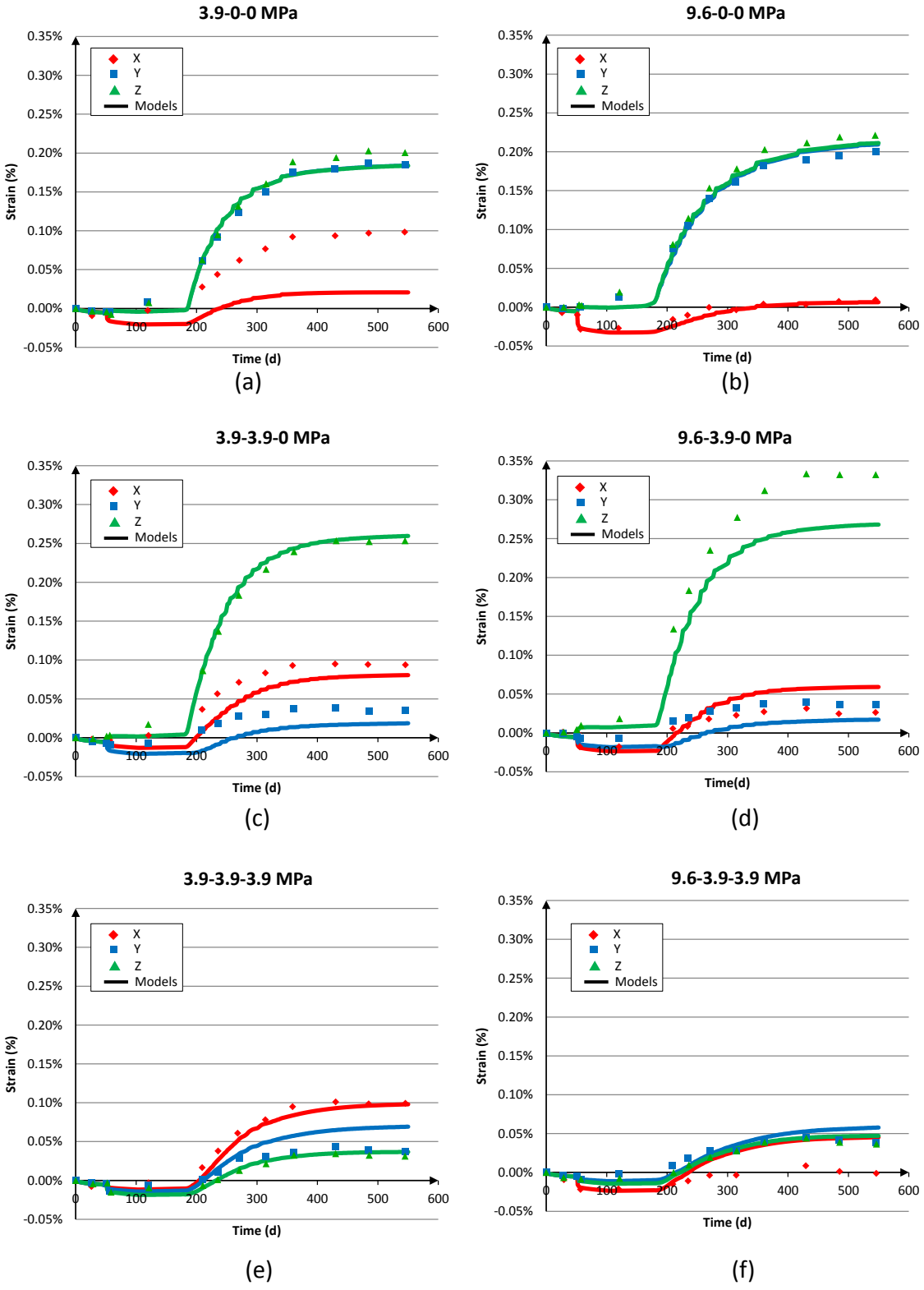

Figure 3.7: Comparison of the experiment results of [2] and the model results: (a) 3.9-0-0 MPa (b) 9.6-0-0 MPa (c) 3.9-3.9-0 MPa (d) 9.6-3.9-0 MPa (e) 3.9-3.9-3.9 MPa (f) 9.6-3.9-3.9 MPa

As mentioned in [11], the stress field is really heterogeneous in these tests. Indeed, in the present modelling, the compressive stress can vary from 0 to 6 MPa in the concrete in the 3.9-3.9-3.9 MPa test. Thus, the strains and displacements fields are really different along the same edge of the structure. Deformed shapes of the 9.6-0-0 MPa and the 3.9-3.9-3.9 MPa tests are respectively represented in the Figure 3-8 and in the Figure 3-9. Large gradients of expansion can be observed between small strain close to the steel plates and the edges of the cube. Structural cracks are obtained numerically in this area. To conclude, the model reproduces faithfully the multi-axial strains but the heterogeneity of the results due to the loading arrangement (especially the contact between steel plates and concrete) question the experimental information used and consequently the numerical benchmarking.

As the loadings are not maintained [2], the steel strains (Figure 3.10) decrease with time due to concrete creep. The losses are respectively 14% and 22% for the 3.9-0-0 MPa and the 9.6-0-0 MPa test. Thus, the compressive stresses applied are not constant during the tests due to concrete relaxation which is not totally counterbalanced by expansion, as already discussed for creep [14, 3]. The strains of concrete directly submitted to compression under the plates are mainly due to creep while the strains of concrete close to the stress free edges are mainly due to ASR expansion. Furthermore, the relaxation in the prestressing bars should also be taken into account in the analysis. As concrete creep modelling is calibrated on the experimental strain, the consideration of steel relaxation could lead to a modification of creep parameters. Therefore, the global strains analysis is complex.

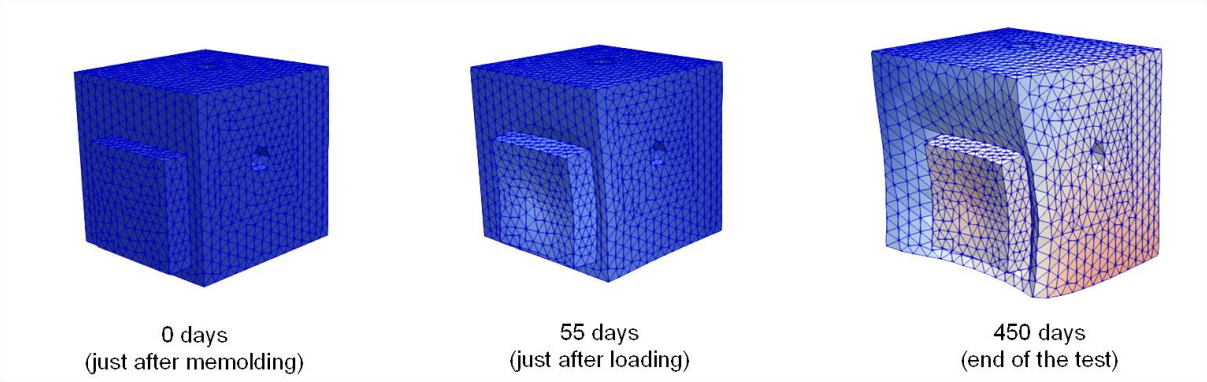

Figure 3.8: Deformed shape at different time for the 9.6-0-0 MPa test

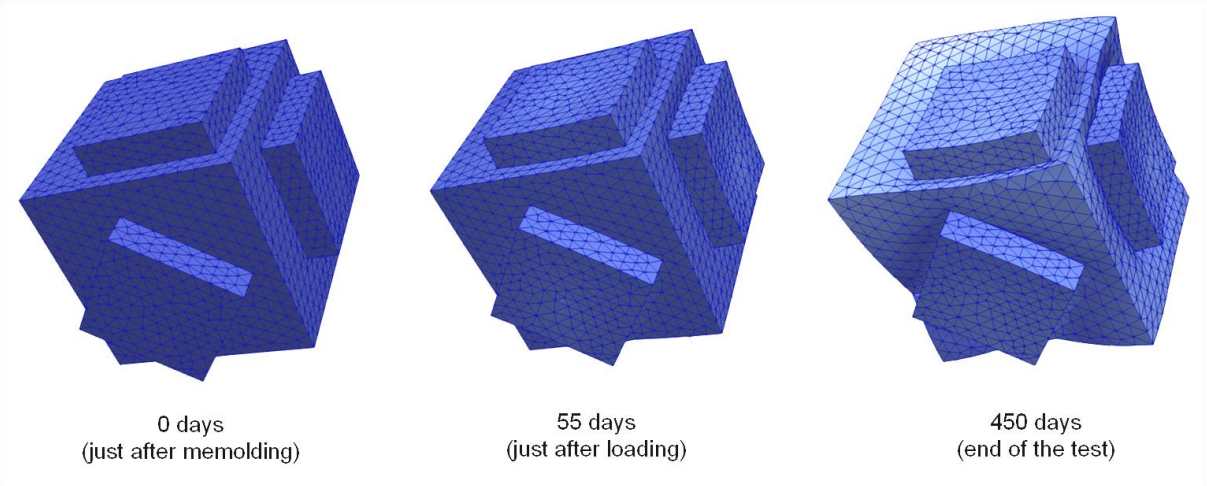

Figure 3.9: Deformed shape at different time for the 3.9-3.9-3.9 MPa test

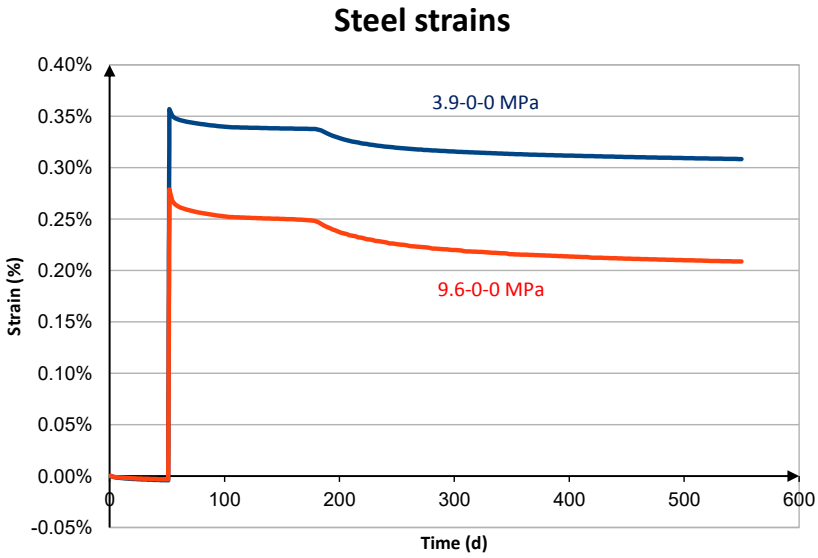

Figure 3.10: Steel strains of the 3.9-0-0 MPa and 9.6-0-0 MPa tests showing the concrete creep

4. CONCLUSION

Alkali-Silica Reaction is a strong source of concern for engineers in charge of affected structures. Most of the time, the concrete is under mutli-axial loadings due to external mechanical loadings or restraints that lead to anisotropic cracking. The expansion can be reduced according to the amplitude of the compressive stress.

An anisotropic poromechanical model which takes into account creep, already validated on ASR submitted to the combination of stress and restraints [4, 9], has been applied to two recent experimental result series obtained on laboratory under triaxial stresses [1, 2]. In these experimental set up, the stresses were applied by post-tensioning bolts or triaxial machine that allow ASR expansion under real multiaxial compressive loading to be obtained. The model calibrations have been done only on stress free expansion. Creep strains of non-reactive samples are available to calibrate the creep parameters separately.

Model results globally reproduce the strains in all the directions faithfully. In the directions of applied loadings, expansion and creep are opposed without total balance as already discussed in the literature.

In the first modelled experiment [1], the stress state is changed during the tests. The model reproduces the measured strains in terms of amplitude and kinetics when the stress is increased in one direction. In the test where the stress is decreased, the model overestimated the response.

In the second modelled experiment [2], the geometry was finally quite complex considering external steel plates, internal prestressed bolts with holes inside the concrete. The location of the plates and the bolts were different for the three directions X, Y or Z. The stress state is strongly heterogenous in the concrete. Furthermore, following the bolts prestressing, the concrete creeps and the compressive stress in the concrete is logically decreasing. Despite these conditions, the model reproduces quite well the strains in all directions.

The model is able to reproduce these two new experimentations with the calibration of the hardening law obtained on Multon's experiments [3, 4]. Only stress free expansion was calibrated in this work. This is possible thanks to the hardening law which is mainly driven by mechanical properties (concrete modulus before diffuse cracking and tensile strength). Only the modulus after diffuse cracking needs to be calibrated (h_g about 0.03), and it seems to be almost the same for all the experimentations available in the literature.

The numerical model validated here can be a tool for engineers that assess the safety of large ASR affected structures. To reproduce the ASR expansions under multi-axial loadings, the model must strongly combine ASR anisotropy expansions and creep.

5. ACKNOWLEDGEMENTS

Dr J. Liaudat is thanked for providing the experimental curves.

6. REFERENCES

[1] Liaudat J, Carol I, López CM, Saouma VE (2017) ASR expansions in concrete under triaxial confinement. Cement and Concrete Composites. https://doi.org/10.1016/j.cemconcomp.2017.10.010

[2] Gautam BP, Panesar DK (2016) A new method of applying long-term multiaxial stresses in concrete specimens undergoing ASR, and their triaxial expansions. Mater Struct 49:3495–3508. https://doi.org/10.1617/s11527-015-0734-z

[3] Multon S, Toutlemonde F (2006) Effect of applied stresses on alkali–silica reaction-induced expansions. Cement and Concrete Research 36:912–920. https://doi.org/10.1016/j.cemconres.2005.11.012

[4] Morenon P, Multon S, Sellier A, et al (2017) Impact of stresses and restraints on ASR expansion. Construction and Building Materials 140:58–74. https://doi.org/10.1016/j.conbuildmat.2017.02.067

[5[Coussy O (1991) Mécanique des milieux poreux. Editions Technip

[6] Morenon P (2017) Modélisation des réactions de gonflement interne des bétons avec prise en compte des couplages poro-mécaniques et chimiques. Université de Toulouse, Université Toulouse III - Paul Sabatier

[7] Poyet S, Sellier, A., Capra, B., et al (2006) Influence of Water on Alkali-Silica Reaction: Experimental Study and Numerical Simulations. Journal of Materials in Civil Engineering 18:588–596. https://doi.org/10.1061/(ASCE)0899-1561(2006)18:4(588)

[8] Grimal E, Sellier A, Multon S, et al (2010) Concrete modelling for expertise of structures affected by alkali aggregate reaction. Cement and Concrete Research 40:502–507. https://doi.org/10.1016/j.cemconres.2009.09.007

[9] Morenon P, Multon S, Sellier A, et al (2019) Flexural performance of reinforced concrete beams damaged by Alkali-Silica Reaction. Cement and Concrete Composites 103412

[10] Sellier A, Multon S, Buffo-Lacarrière L, et al (2016) Concrete creep modelling for structural applications: non-linearity, multi-axiality, hydration, temperature and drying effects. Cement and Concrete Research 79:301–315. https://doi.org/10.1016/j.cemconres.2015.10.001

[11] Gautam BP, Panesar DK, Sheikh SA, Vecchio FJ (2017) Multiaxial Expansion-Stress Relationship for Alkali Silica Reaction-Affected Concrete. ACI Materials Journal 114:

[12] Berra M, Faggiani G, Mangialardi T, Paolini AE (2010) Influence of stress restraint on the expansive behaviour of concrete affected by alkali-silica reaction. Cement and Concrete Research 40:1403–1409. https://doi.org/10.1016/j.cemconres.2010.05.002

[13] Kawamura M, Iwahori K (2004) ASR gel composition and expansive pressure in mortars under restraint. Cement and Concrete Composites 26:47–56. https://doi.org/10.1016/S0958-9465(02)00135-X

[14] Larive C (1997) Apports combinés de l'expérimentation et de la modélisation à la compréhension de l'alcali-réaction et de ses effets mécaniques. PhD thesis, Ecole Nationale des Ponts et Chaussées